A&A 386, 42–59 (2002)
DOI: 10.1051/0004-6361:20020045

Astronomy & Astrophysics

Fabry-Perot observations of the ionized gas in the spiral galaxy NGC 6951

M. Rozas[1,2], M. Relaño[1], A. Zurita[1], and J. E. Beckman[1,3]

[1] Instituto de Astrofísica de Canarias, E-38200 La Laguna, Tenerife, Canarias, Spain
[2] Observatorio Astronómico Nacional (UNAM), Ensenada, B.C., México
[3] Consejo Superior de Investigaciones Cientificas, Spain

Received 27 November 2000 / Accepted 2 January 2002

Abstract. We present two dimensional kinematic observations at high angular and velocity resolution measured via the Hα emission line in the active barred spiral NGC 6951, obtained using the TAURUS II Fabry-Perot system on the 4.2 m William Herschel Telescope. From the radial velocity map we produced the rotation curve, which has a rapidly rising inner portion, and then remains remarkably flat to large radii. Subtracting a two-dimensional projected model of this rotation from the observed map yields a residual velocity map which shows significant non-circular motions, above all in the circumnuclear zone, where they reach projected values of 45 km s^{-1}. The kinematic and morphological properties of this zone, a narrow well-defined annular region, point to inflow of gas resulting from perturbation in the stream-lined gas flow due to the bar, as predicted in dynamical models. The overall gas kinematics leads us to infer the presence of an inner disc within the main galactic disc, whose presence is marked by two inner Lindblad resonances at 180 pc and 900 pc from the centre respectively. Our map of the Hα velocity dispersion shows characteristic values of 20 km s^{-1} for the HII regions, and an obvious correlation between higher values and the brightest HII regions. The value rises to >100 km s^{-1} as the nucleus is approached.

Key words. galaxies: individual: NGC 6951 – galaxies: spiral – ISM: HII regions

1. Introduction

The possible relation between active galactic nuclei (AGN) and the starburst phenomenon in galactic circumnuclear zones has been widely treated in recent years. In this context there is a special interest in studying those galaxies in which nuclear activity and violent star formation are both observed. Arsenault (1989) showed a correlation between the presence of circumnuclear rings of star formation and nuclear activity, though the physical connection between them was not clear. It is also clear that one should not try to interpret nuclear activity without considering the framework of the host galaxy (see e.g. Moles et al. 1986). We have chosen to observe NGC 6951, a barred spiral with active star formation and also nuclear activity, with these problems in mind. It is noteworthy that in those spirals which contain bright circumnuclear hot spots, such as NGC 6951, the presence of these and other distinctive features shows a strong tendency to be related to the presence of a bar. In their pioneering study of this phenomenon, Sersic & Pastoriza (1967) found that in a quite sizeable sample of 174 bright galaxies, all the cases of striking circumnuclear morphology occur in galaxies which are either barred, SB, or mixed SAB. In a comprehensive follow up to this programme, Buta & Crocker (1993) put together an extensive catalogue of galaxies with "nuclear rings", in which many of the cases of circumnuclear star formation are located in localized hot spots which collectively form a kiloparsec scale ring or spiral pattern around the nucleus. Theoretical modelling studies suggest that star-forming annular zones should develop in those barred galaxies where gas, plus dust, flow inwards from an inner Lindblad resonance (ILR), or between two ILR's (Combes & Gerin 1985; Knapen et al. 1995; Ho et al. 1997). Multi-wavelength studies of these objects have shown that these rings are sites of intense star formation, with high supernova rates (Hummel et al. 1987; Wilson et al. 1991; Forbes et al. 1994b). A review of observations of nuclear hot spots can be found in Kennicutt (1994).

The kinematics of the circumnuclear zone is often more complex than the large-scale disc kinematics, due to a combination of factors: (a) gas flows induced by non–axisymmetric potentials, e.g. due to bars, which alter the mass distribution around the centre far more than in other zones; (b) the formation of multiple resonances; (c) possible nuclear activity, induced by the mass concentration. However in order to understand fully the circumnuclear kinematics, one must consider it in the context

Send offprint requests to: M. Rozas,
e-mail: maite@astrosen.unam.mx

of the dynamics of the whole galaxy. There is observational evidence, supported by theoretical models, that significant mass redistribution can occur within galaxies on timescales short compared with the Hubble time (Friedli & Martinet 1993; Berentzen et al. 1998). This can occur via processes internal to the galaxy, associated with non–axisymmetric components of the gravitational potential, and more readily if there is an external torque, which can exert a powerful influence, above all on the gas components of discs, but also on their stellar components (Shlosman 1990; Zhang 1996; Combes 1988). Barred galaxies show frequent evidence of secular dynamical evolution; they often show "starburst" activity in their central zones, with well marked circumnuclear regions of star formation (Kennicutt 1994; Buta & Combes 1996), on ∼1 kpc scales. High resolution imaging in emission lines notably in Hα reveal these inner structures, which can also be detected via interferometry in their molecular emission via CO, and where adequate resolution can be applied, even at 21 cm in HI.

The evolution of these circumnuclear regions can be followed by combined observations of a number of key parameters, which allow us to study the rate of inflow of gas along the bar, the star formation efficiency in the circumnuclear zone, and the dynamical effects of the gas and stars accumulating around the nucleus. These parameters include the surface densities of the gas components, the surface emissivity of the ionized gas, and the velocity fields both in gas and stars (the former shows the direct gas response to all the gravitational influences, and the latter can provide the underlying potential). The best way to proceed is in fact to measure the relevant parameters not only with the inner 1 kpc but also out along the bar and into the disc. With these ends in view, we planned observations of the ionized gas in NGC 6951 via Hα emission, using Fabry-Perot interferometry. This technique permits us to obtain kinematic information across the whole face of a galaxy at once; it offers a three-dimensional "data cube" of intensity versus position in each of a set of discretized wavelength channels, from which moment maps of integrated intensity, radial velocity, and velocity dispersion along the line of sight can be extracted. From this data set we can use the ionized hydrogen as a tracer of star formation, and of velocity fields within and perpendicular to the plane of the galaxy, as well as dynamical processes within individual star forming zones. The types of velocity fields anticipated include "streaming motions" across spiral arms, or gas flows in the direction of the major bar axis; measurements of these fields allow us to infer the response of the gas to the underlying potentials involved (cf. Knapen et al. 1997; Rozas et al. 2000). The technique for this is to assume symmetry in the underlying rotation curve, and first order reflection symmetry in the rest of the velocity pattern; the rotational curve is then subtracted from the observed field, and the residual field enables the non-circular components to be fairly well estimated. It is also possible to use the data cube to extract the point by point velocity dispersion map, from which the internal motions of dynamically active regions, and any velocity components perpendicular to the plane of the galaxy may be derived (see Combes & Becquaret 1997; Rozas et al. 1998).

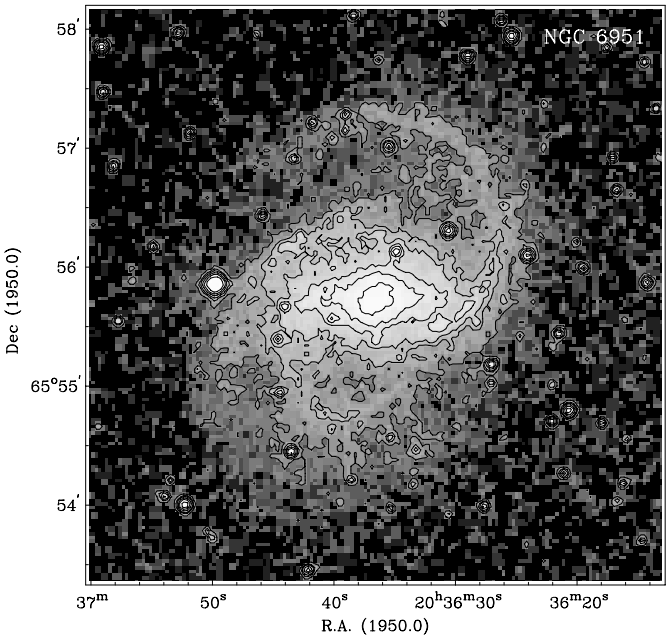

Fig. 1. Optical image of NGC 6951.

In the present article we apply this technique to study kinematically the barred active spiral NGC 6951 from a "TAURUS" Fabry-Perot map of NGC 6951. In Sect. 2 we give a descriptive summary of the previously measured properties of the galaxy, in Sect. 3 we detail the observations, their reduction, and the preliminary analysis, in Sect. 4 we analyze the brightness distribution of the emitting ionized gas, in Sect. 5 we analyze the velocity distribution, in Sect. 6 we go into more depth in a treatment of the circumnuclear region, and in Sect. 7 we set out our conclusions.

2. NGC 6951

NGC 6951 is a spiral galaxy, classified as SAB(rs)bc (de Vaucouleurs et al. 1991), which has a large stellar bar revealed by near-infrared photometry (Mulchaey et al. 1997; Friedli et al. 1996; Elmegreen et al. 1996) and distorted spiral arms (see Fig. 1)[1]. Its central zone is compact and highly ionized, and surrounded by an annulus formed by bright HII regions (Buta & Crocker 1993). Measured line ratios in the nuclear zone are

[1] Based on photografic data of the National Geographic Society–Palomar Observatory Sky Survey (NGS-POSS) obtained using the Oschin Telescope on Palomar Mountain. The NGS–POSS was funded by a grant from the National Geographic Society to the California Institute of Technology. The plates were processed into the present compressed digital form with their permission. The Digitized Sky Survey was produced at the Space Telescope Science Institute under US Government grant NAG W-2166.

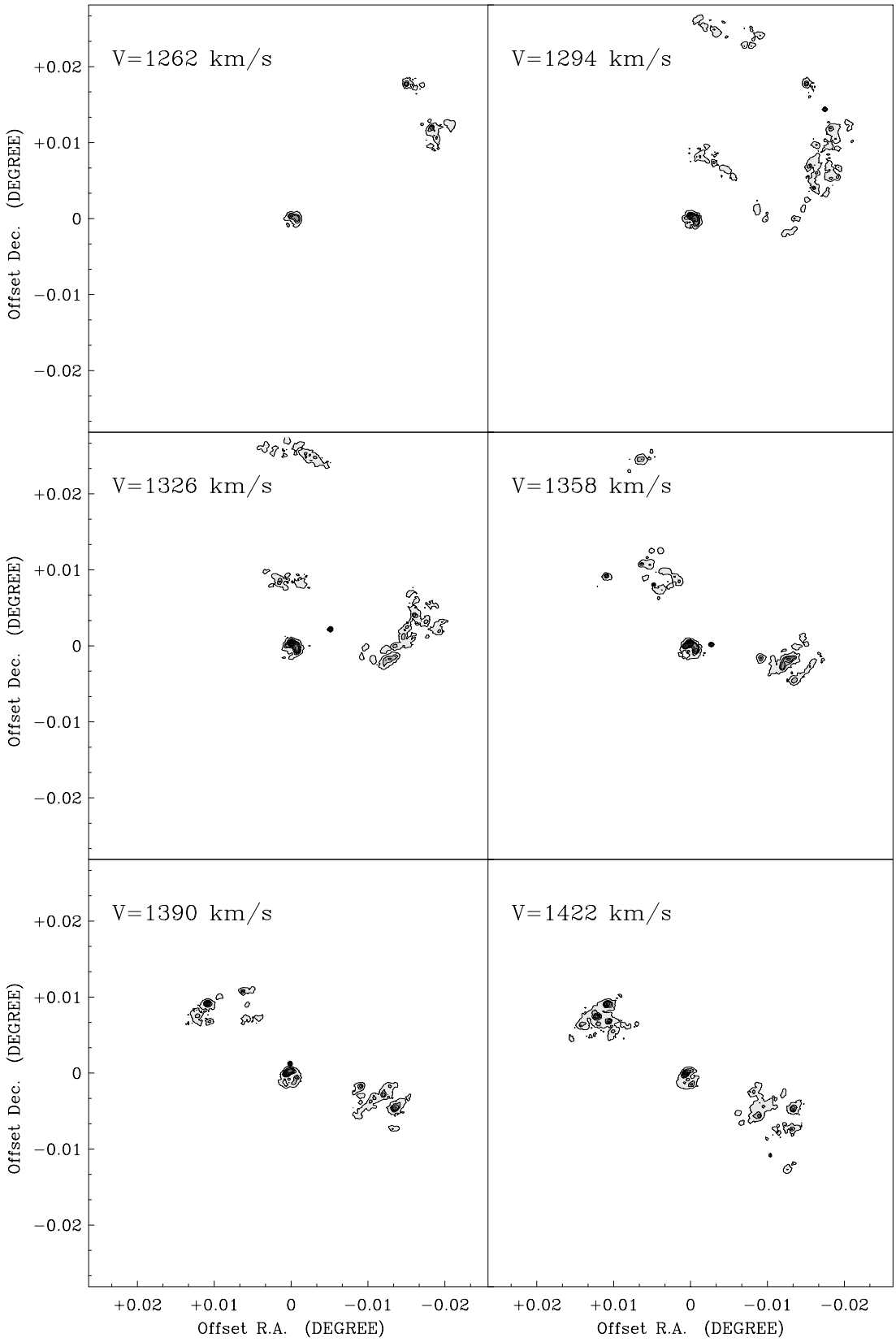

Fig. 2. Planes of the Hα high resolution (1.3″) data cube for NGC 6951 (before "cleaning" the data cube; see text for details) at a series of velocities about the central systemic value of 1422 km s^{-1}.

pointers to activity; the nucleus has been classified as Seyfert 1, Seyfert 2, and Liner (Filippenko & Sargent 1985; de Robertis & Osterbrock 1986; Depree et al. 1991). Filippenko & Sargent (1985) pointing out that the ratio

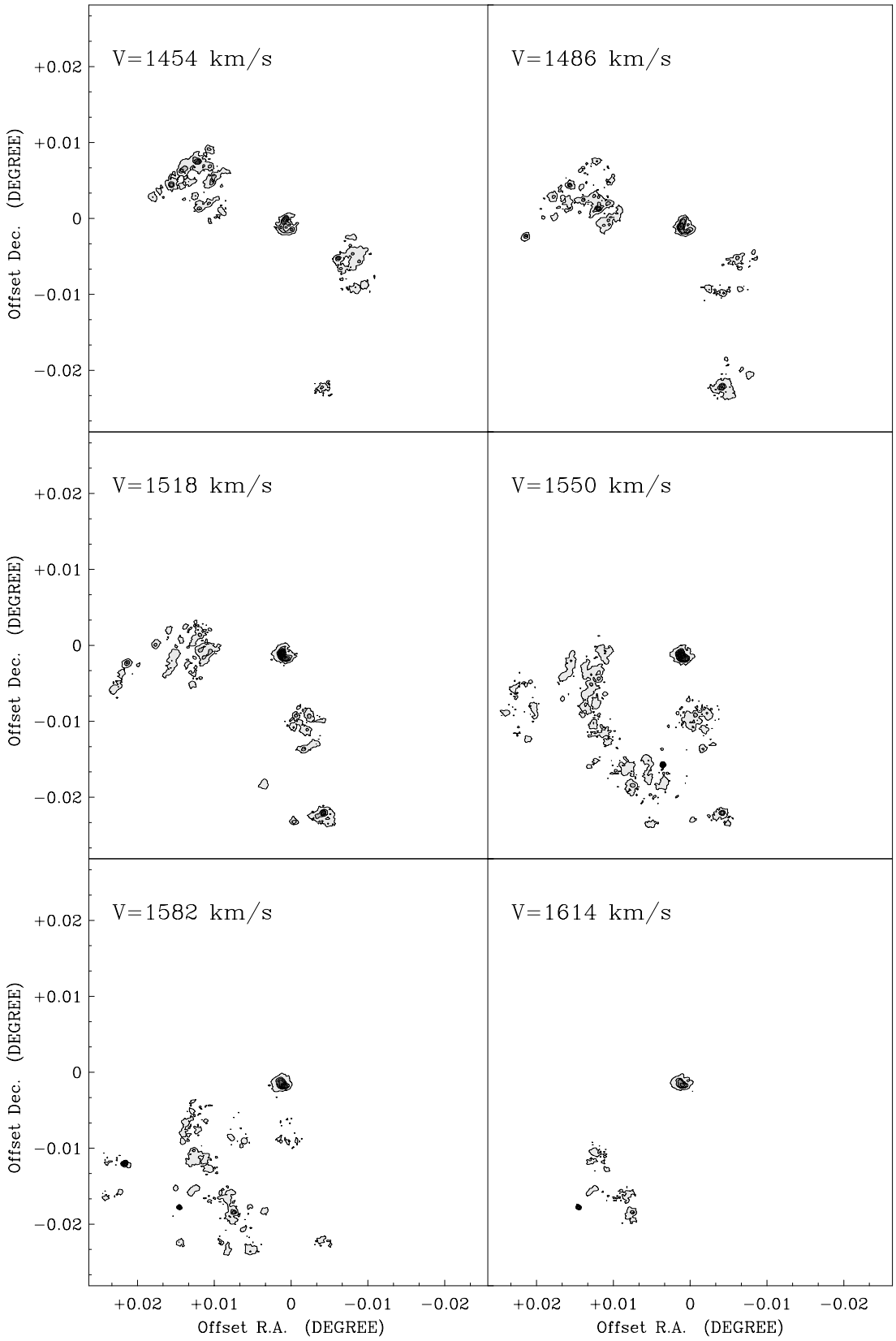

Fig. 2. continued.

of [NII]/Hα reaches values of 3 at the nucleus, falling to values less than 1 in the HII regions in the ring. Values significantly greater than unity are characteristic of active nuclei, while values less than 1 characterize HII regions in general. The radial decline in the [NII]/Hα ratio was confirmed by Muñoz-Tuñón et al. (1989), who found

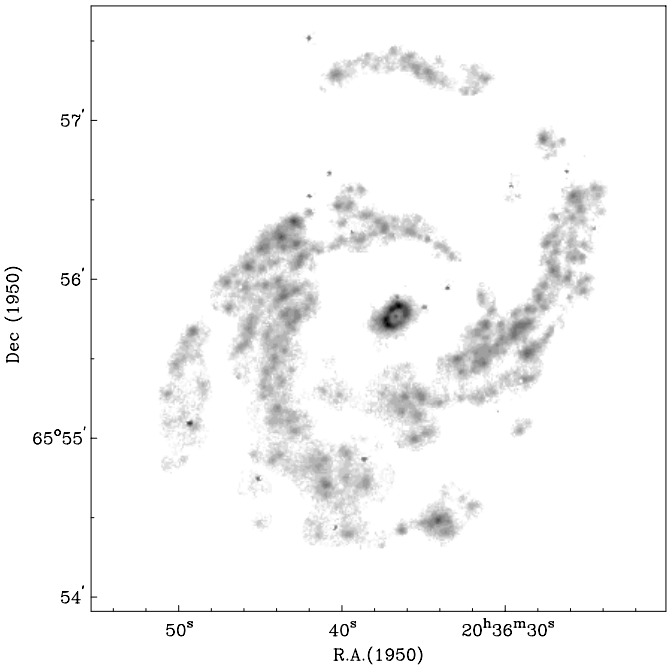

Fig. 3. Intensity map (zeroth moment) of the Hα emission in NGC 6951 obtained with the high resolution (1.3″) Hα data cube.

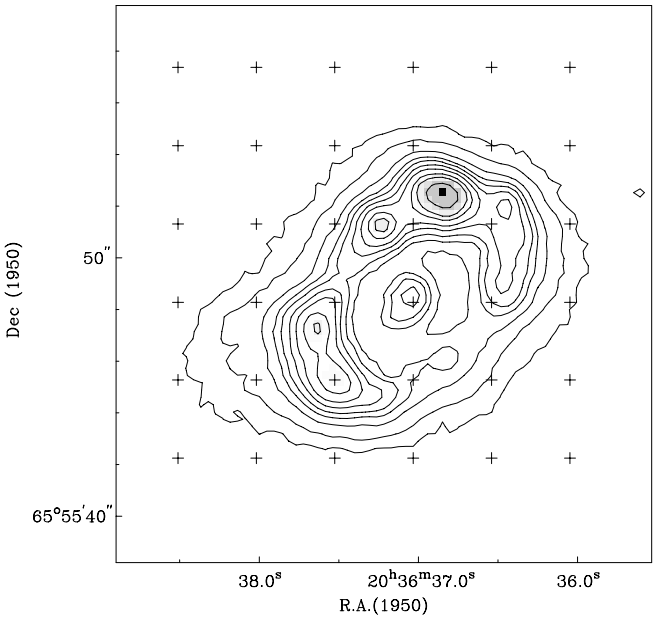

Fig. 4. Integrated intensity map of Hα emission in the central region of NGC 6951. The contour levels are 5, 6, 7... 15σ. The grid positions in the line profile map (Fig. 5) are indicated here by crosses.

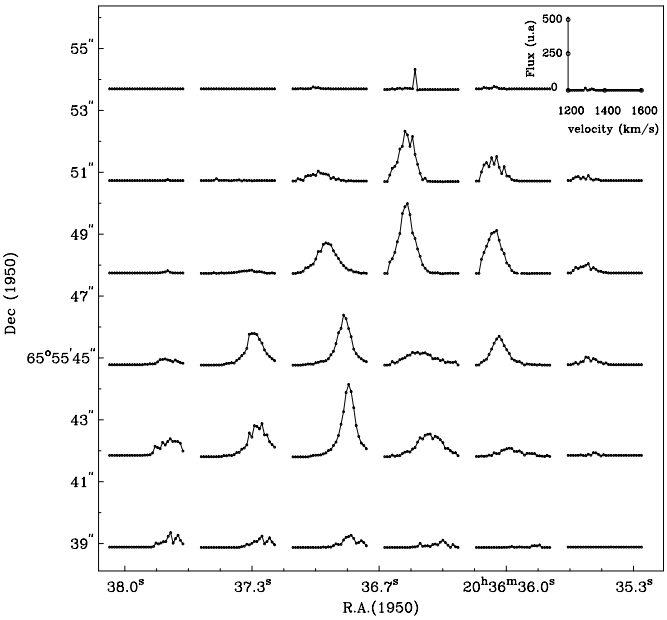

Fig. 5. Line profile map of the Hα emission derived from the full resolution data cube of the central region of NGC 6951. The line profiles were measured at 6×6 points on the 3″ spacing $\alpha - \delta$ grid. The width of a velocity bin is 15.69 km s^{-1} .

values close to 4 in the central arcsecond, falling to 0.2 at 20 arcsec from the centre. In fact the nucleus has been classified as a Seyfert 1 (de Robertis & Osterbrock 1986) or a Seyfert 2 (Depree et al. 1991), and this second option seems now to be confirmed by Ho et al. (1997) with the most accurate study to date performed, with high data quality and good correction for underlying absorption. Finaly, Pérez et al. (2000) suggest that the nucleus in NGC 6951 can be considered as a transition object between a very high excitation Liner and a possible nitrogen overabundant Seyfert 2. Its general optical and kinematic properties have been covered in papers by Márquez & Moles (1993), Boer & Schulz (1993) and Rozas et al. (1996). The CO and Hα emission within 10 arcsec of the nucleus show a twin–peaked structure (Kenney et al. 1992) which suggests the presence of a two armed spiral or a broken ring. Radio frequency maps by Saikia et al. (1989) and by Vila–Vilaró et al. (1990) also show a two–component structure, but with extended emission extending from 5 arcsec SE to 5 arcsec NW of the nucleus, with a compact central peak.

Near infrared imaging has brought out clearly the presence of a stellar bar with a semimajor axis of 44 arcsec (Friedli et al. 1996; Elmegreen et al. 1996; Mulchaey et al. 1997), which can in fact be picked out in optical images. In Fig. 1 we show a V-band image of the galaxy, in which some of its main large scale features can be seen: two non-symmetric spiral arms emerge from the ends of a major EW bar structure. The southern arm is less well defined than its northern counterpart. The internal isophotes show distorsions related to the dust lanes parallel to the bar, but which cut it within the circumnuclear zone (Kenney et al. 1992; Márquez & Moles 1993; Wozniak et al. 1995). These dust lanes trace the shock front in the gas towards the edges of the bar, predicted by theoretical models (Roberts et al. 1979; Athanassoula 1992).

It is worth noting that NGC 6951 is remarkably isolated. It is conventionally claimed that galaxies with active star formation are interacting with others (Adams 1977; Dahari 1985; Joseph et al. 1984; Joseph & Wright 1985; Laurikainen & Moles 1988, 1989). However there is

no theoretical reason why an isolated galaxy should not show such activity. We have searched the CfA catalogue, and found that there are no detected objects within 1 Mpc of NGC 6951, nor within a redshift of 500 km s^{-1} of it, so that we can infer that no significant gravitational interaction with a neighbour galaxy has occurred for the past 10^9 years. We have summarized the key observational parameters for the galaxy in Table 1.

Table 1. NGC 6951: basic parameters.

Parameter	Value	Reference
Type	SAB(rs)bc	1
Nuclear activity	Seyfert 2	2
RA (1950)	$20^h36^m36^s.59$	3
Dec (1950)	$65°55'46''$	3
$D_{25} \times d_{25}$	3.9×3.2	1
Inclination angle	42°	4,5
Position angle	137°	4
Accepted distance	24.1 Mpc	6

(1): de Vaucouleurs et al. (1991); (2): Ho et al. (1995); (3): Saikia et al. (1994); (4): this work; (5): Márquez & Moles (1993); (6): Tully (1988).

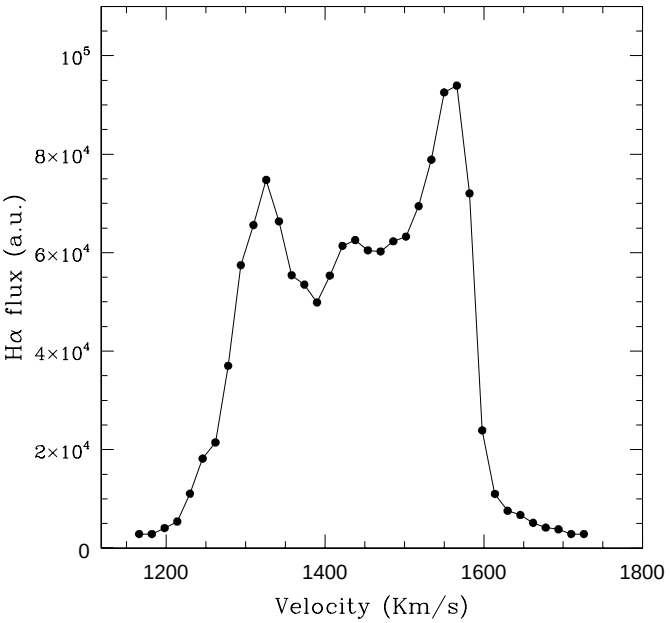

Fig. 6. Integrated Hα profile of NGC 6951.

3. Observations and data reduction

We used the TAURUS II camera in scanning Fabry-Perot mode, at the Cassegrain focus of the 4.2 m William Herschel Telescope at the ORM observatory La Palma, during the nights of March 26th and 27th 1996. The 125 μ etalon, and f/2.11 camera were employed, together with a TeK CCD, windowed to a size of 500×500 pixels, each pixel having an effective size of $0.56'' \times 0.56''$. The nights were photometric, and the seeing had a mean value of $1.1''$.

The observations with TAURUS take the form of a series of images each in a narrow wavelength interval, the whole set covering the emission line in Hα emitted by the galaxy. A narrow-band filter with the appropriate red-shift ($\lambda_0 = 6589$ Å, $\Delta\lambda = 15$ Å) isolates the Hα emission line; the wavelength was selected according to the recession velocity of the galaxy (1426 km s^{-1} from RC3), and the filter serves not only to cut out contributions from the nearby lines of the [NII] doublet, but also to eliminate other orders of the interferometer. The whole "data cube" comprising 55 wavelength planes, with 140 s exposure time per plane, covered a full spectral range of 17.22 Å or the equivalent of 790 km s^{-1}. A "calibration cube" using a CuNe emission lamp was taken at the beginning of the night, and "calibration rings" before and after the data cube exposure on the galaxy. These were later used for phase and wavelength calibration of the data cube using the TAUCAL software package. After calibration the raw data cube, in which the surfaces of constant wavelength are paraboloids, was converted to a Cartesian cuboid of 55 planes, separated by 0.34 Å each of 500×500 pixels. After this we subtracted off the sky emission from each plane separately, and the planes were aligned using field stars. The next step was the astrometric relation of the positions of the HII regions with respect to these stars, using a high resolution Hα image of NGC 6951 taken previously (Rozas et al. 1996a). The final reduced data cube had an effective angular resolution of $1.3''$.

With the reduced cube, we could apply MOMENTS, a set of tasks in the GIPSY suite of programmes, to produce moment maps which contain desired information about the intensity and velocity distributions implicit in the individual channel maps (i.e. the plane by plane information shown in Fig. 2). MOMENTS enabled us to calculate the zero, first and second order moments of the intensity in each pixel, which yield the intensity, velocity and velocity dispersion maps respectively. In performing these procedures we rejected as signal any bright pixel which was not reproduced in at least three adjacent wavelength planes. An initial inspection of the moment maps first obtained in this way revealed that the integration over the full velocity range had resulted in noise peaks, so that we had to revise the original data cube to find a method to minimize the effects of this noise. The procedure used for cleaning the cube is exactly that used for the equivalent data in NGC 3359, as described in detail in Rozas et al. (2000), using derived cubes at angular resolution $10''$, $6''$ and $3''$.

The emission in Hα as a function of wavelength channel, i.e. as a function of velocity, for the high resolution cube is shown in Fig. 2, as a set of "channel maps", following radioastronomical practice. The emission is presented in the central $40'' \times 40''$ (4.2 kpc $\times$ 4.2 kpc). We detected significant Hα emission in 33 channels, corresponding to a velocity range from 1214 to 1646 km s^{-1}. This range is comparable to that detected in CO and HCN by Kohno et al. (1999), although the Hα emission is much stronger

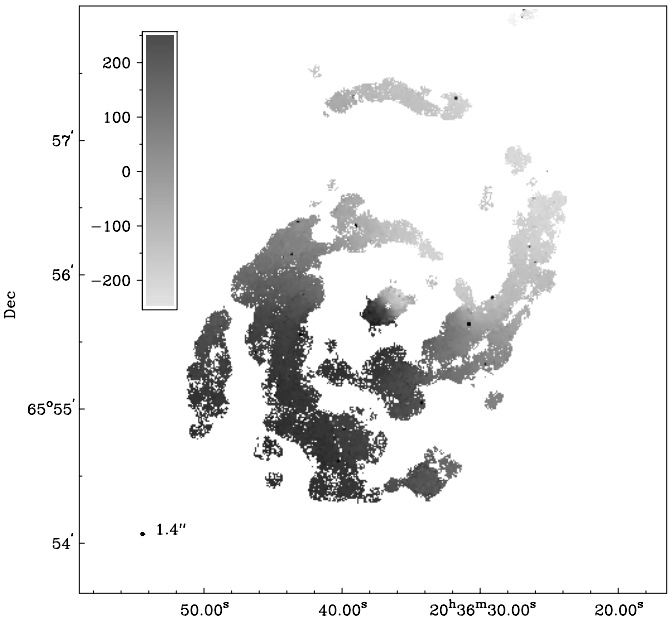

Fig. 7. High resolution (1.3″) velocity map for NGC 6951. The darker zone is the receding side (positive redshift) and the lighter part is the approaching side of the galaxy. The kinematical centre is marked with an asterisk.

in the centre, i.e. in the circumnuclear zone, than the CO or HCN emission.

The intensity, velocity, and velocity dispersion maps, obtained as moments of the data cube as outlined above, were the key results of the initial reduction. The high resolution (1.3″) intensity and velocity maps are shown respectively in Figs. 3 and 7. There are in fact two possible approaches to produce these maps, one via the moments method, and the other by fitting the data within a given resolution element by a Gaussian in the velocity dimension. The resulting velocity maps were essentially the same for both methods, but there were notable differences in the intensity maps and above all in the velocity dispersion maps obtained using the two different techniques. This is because the moments method can lead to significant information loss in the line wings if these have low intensity and high velocity dispersion (van der Kruit & Shostak 1982). This is a result of the noise threshold, a fixed multiple of the measured rms noise, which leads to a cut-off level below which the information is deemed not to be significant. In the Gaussian profile method, the cut-off applied is a function of the signal strength itself, and is not a fixed level, which allows more sensitive detection of line wings, but may lead to a problem of treating noise as low level spurious signal in noisy images. In the present study we have chosen to use the moments method, knowing its limitations. A fuller analysis of the map of velocity dispersion, investigating the internal kinematics of the HII regions, and comparing both methods to obtain the full spectra of velocities over the full HII region population, together with the relation of the velocity dispersion in the principal component to the HII region luminosity will be presented in Relaño et al. (2001).

4. Distribution of the ionized gas

In Fig. 3 we show the map of the line intensity in Hα which brings out the brightest HII regions. Previous observations in the visible (Márquez & Moles 1993; Wozniak et al. 1995; Rozas et al. 1996a, b; González–Delgado et al. 1997) and in radio continuum emission at 6 cm. Vila et al. (1990) and Saikia et al. (1994) show that the emission is mainly concentrated in the central zone of the galaxy, within a few hundred pc of the nucleus. All these observations indicate vigorous star formation in a zone of some $6'' \times 9''$ around the nucleus (Barth et al. 1995; Buta & Crocker 1993). This zone contains giant complexes of HII regions, which are much more luminous than the majority of regions. Outside this zone the Hα emission is symmetrically distributed principally in the spiral arms. A more detailed map of the Hα emission in the circumnuclear zone is shown in Fig. 4.

We have used our calibrated photometric Hα image, previously presented in Rozas et al. (1996a), together with an estimated extinction, extrapolated from the visual value $A_v = 3.4$ mag (Barth et al. 1995), to estimate the luminosity in Hα of the circumnuclear zone at 4.3×10^{41} erg s^{-1}. Of this luminosity only a tiny fraction (some 1%) comes from the nucleus. The star formation rate can be determined, assuming a standard IMF, using the relation: $L(\mathrm{H}\alpha\ )/1.12 \times 10^{41}$ erg s^{-1} (see Kennicutt 1983), which gives 3.9 $M_\odot$ yr^{-1} for this zone. This is a value typical of nearby starburst galaxies.

In Rozas et al. (1996a,b) we analyzed the physical and statistical properties of the HII regions of NGC 6951, cataloguing 674 regions with luminosities above our detection limit, of which 603 are in the spiral arms, and 71 in the interarm zone, and measuring their sizes and Hα luminosities. The luminosity function follows a power law: $\mathrm{d}N(L) = A L^{\alpha}\ \mathrm{d}L$ where $\alpha = -2.21(\pm 0.1)$, coinciding with the values found for other galaxies of comparable morphological type (Kennicutt et al. 1989; Rozas et al. 1996a,b; 1998). The radial dependence of the mean Hα surface brightness, found by dividing the total emission in rings of equal radial interval by the area of each respective ring, is shown in Fig. 6, which brings out the dominance of the circumnuclear emission.

In Fig. 5 we show a set of emission line profiles corresponding to the innermost zone of the galaxy. These data, taken from the high resolution cube, are plotted on a grid with 3 arcsec spacings in both RA and Dec. These grid points are marked with crosses in the Hα intensity map of Fig. 4. This zone contains two principal emission intensity peaks, which lie on an oval annulus of enhanced emission, centred on the nucleus with semiaxes of 6 arcsec and 4 arcsec. These peaks show up also in the emission by the CO molecule, as demonstrated by Kenney et al. (1992), who postulated that these peaks might correspond to crowded orbits in the gas near the multiple Lindblad resonances, whose presence can be inferred from the behaviour of the rotation curve in the range of nucleocentric radii concerned. The presence of twin intensity peaks in

the molecular gas was confirmed by Kohno et al. (1999), who made detections in CO and also in HCN. In fact our Hα peaks coincide in position with Kohno et al.'s (1999) HCN peaks rather than with the peaks in the CO. The presence of strong HCN emission in regions with strong star formation has been shown in characteristic nuclear starburst galaxies such as M 82 (Shen & Lo 1995) and NGC 253 (Paglione et al. 1995b)

5. Global kinematics

In the Hα channel maps shown in Fig. 2 the general scheme of the rotating galaxy can be followed in its global velocity characteristics. Integrating the emission in each channel yields the integrated velocity profile shown in Fig. 6, which shows a double–peaked structure similar to that found for many rotating spirals in HI and which is also well seen in the HI profile of this object measured by Haynes et al. (1998). In Hα however, there is more emission at the systemic velocity because of the strong circumnuclear emission zone, while does not have an HI counterpart. The asymmetry in Fig. 6, much more pronounced than in HI, reflects the fact that the southern arm and disc show higher surface brightnesses than the northern arm and disc, even though in the south the arm structure is less well defined geometrically.

5.1. The velocity map

In Fig. 7 we give a visual representation of the velocity map of the Hα emission across the face of NGC 6951, calculated using the MOMENTS package in the GIPSY program suite. The map shows the first moment of the emission in each pixel where Hα is detected, which is equivalent to the global velocity distribution. A characteristic of the ionized gas distribution in a galaxy, which implies a certain inconvenience in using Hα as velocity tracer, is its patchy structure, which is readily seen in Fig. 7, and which contrasts with the relatively smooth distribution typical of HI. To handle the global velocity it is convenient to reduce the effective resolution in the map, and a version smoothed to 10 arcsec is presented in Fig. 9, which allows us to produce relatively regular isovelocity contours superposed on the greyscale map. These contours do not indicate major departures from circular motion in the disc, although there is a hint of systematic kinkiness across the arms which would be expected of streaming motions. The continuously distributed Hα emission in the central zone of NGC 6951 allows us to produce a velocity map of this zone at our full angular resolution, which is shown in Fig. 8. The overall velocity field shows the "spider pattern" expected of a rotating disc having rapidly rising circular velocity with increasing radius. There are, however, significant departures from this pattern, which we will analyze in detail below. There is no indication of warping over the disc as a whole since the kinematic major axis is essentially rectilinear over the whole mapped field, but our observations reach relatively limited radii, and are not especially well suited for detecting warps.

5.2. The rotation curve

The circular velocity in a rotating galaxy is normally plotted via a rotation curve, in which the aim is to minimize any contributions from non–circular components. We have used our Hα cube to plot rotation curves at different angular resolutions. The details of the procedure chosen can be found in Begeman (1989), (also see Rozas et al. 2000). To describe this briefly, the method adjusts a set of parameters describing the velocity field in a series of concentric elliptical annuli about the galactic centre. The parameters are the inclination angle: i, the major axis position angle: PA, and the rotational velocity itself: $V_{\rm c}$. The fits use a least squares algorithm, which requires as additional inputs the systemic velocity of the galaxy: $V_{\rm sys}$, and the coordinates of the centre ($x_{\rm c}$ and $y_{\rm c}$) and utilizes the expression:

$$V = V_{\rm sys} + V_{\rm c} \cos(\theta) \cos(i) \quad (1)$$

where θ is the azimuthal angle in the plane of the galaxy, measured from its major axis. To allow for the effect of projection, points on each annulus are weighted by $\cos(\theta)$ and points within 20 degrees of the minor axis are eliminated.

To find the kinematic centre, which is determined only by the symmetry of the velocity field, we first used the map at $10''$ resolution, taking fixed values, $i = 42°$, PA $= 138°$ and $V_{\rm sys} = 1418$ km s^{-1} (all these values from Márquez & Moles 1993). The results were RA (1950) = 20h36m36.49s and Dec (1950) $= 65°55'46.2''$. These values were obtained using annuli of width 20 arcsec in which the numbers of independent data points were large, so that the resulting errors should be small. This kinematic centroid coincides well with the position of the Seyfert nucleus inferred by Saikia et al. (1994), defined via the peak in the 6 cm radio continuum emission.

The second step was a fine adjustment of the systemic velocity of the galaxy. To do this we used the fixed position of the kinematically derived centre, and inclination angle $i = 42°$, obtaining a value of 1422 ± 0.7 km s^{-1}, which coincides satisfactorily with the value of 1418 km s^{-1} found by Márquez & Moles (1993), and with that given by Boer & Schulz (1993) of 1425 km s^{-1}. This value also agrees well with the value used in the calibration procedure, and although this may appear redundant, during this procedure we in fact varied the values of i and $V_{\rm c}$, finding that the best fits occurred for $i = 41°$–$42°$, and choosing $42°$ finally since this agreed with the value found elsewhere in the literature. In fact we used a constant value of i for the whole disc, in the absence of any evidence for a warp.

After determining the kinematic centre, the systemic velocity, and the inclination angle, we obtained rotation curves for the disc as a whole, and also separately for the approaching and receding halves, using data cubes at different angular resolution and annuli of different widths.

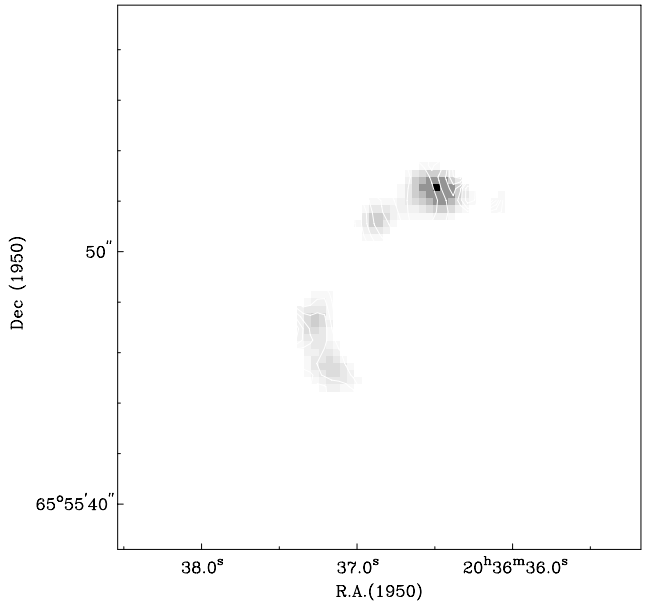

Fig. 8. Hα velocity field of the circumnuclear region of NGC 6951 at full resolution, overlaid on a gray-scale representation of the Hα total intensity, or moment zero, map of the same region. Contours are separated by 15 km s^{-1}.

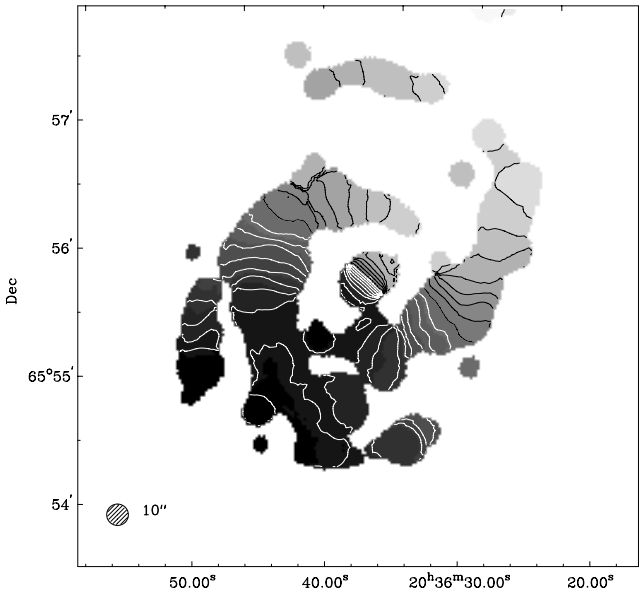

Fig. 9. Low resolution velocity map for NGC 6951 (10″) presenting more clearly the global kinematics of the galaxy. The kinematical centre is marked with an asterisk and isovelocity contours are overlaid on the velocity map. See the text for details of how the map was produced.

In Fig. 10 we show the rotation curve finally adopted (after a second fit taking into account the non-circular motion in the central zone of the galaxy which is described below), using the cube of highest resolution and rings of width 1″. The radial range between the circumnuclear star forming zone, and the spiral arms has very little emission in Hα so in this range only we used the map smoothed to 6″ and a ring width of 4″. In the upper panel of Fig. 10 we show the rotation curve of the full disc, and in the lower panel we show the position angle of the major axis for each ring, measured from North through East, plotted against galactocentric radius.

We can see from the rotation curve that the rotational velocity at large radii takes values between 220 km s^{-1} and 230 km s^{-1}, in agreement with the values found by Márquez & Moles (1993), and with the synthetic curves given by Rubin et al. (1985), for galaxies of similar luminosity and morphological type. The portion of the curve which follows the behaviour of a rigid body extends to 7 arcsec (700 pc) from the nucleus and reaches at this radius a local maximum of 247 km s^{-1}. This distance is within the range in which the bulk of the Hα emission from the circumnuclear annulus is emitted. These values are consistent with the classification of NGC 6951 as a galaxy of intermediate morphological type (Brosche 1971; Baiesi-Pillastrini 1987). We note particularly the very rapid rise in velocity near the nucleus; it reaches values of ∼180 km s^{-1} at 400 pc from the centre, which must in practice mark a lower limit to the velocity gradient (Sofue 1997b). Sofue (1996, 1997b) show that the nuclear CO rotation curves generally rise more sharply in the central few hundred parsecs than those derived from HI and optical observations alone. Rubin et al. (1997) have also shown that the central rotation curves rise steeply within a few hundred pc, indicating a massive rotating disk around the nucleus. We checked to see whether this rise could possibly be due to an instrumental effect, and in particular to a possible inaccurate subtraction of the continuum over the central region of the galaxy. This was done by setting the values of pixels to "blank" in an area of 2″ and 4″ in the continuum-subtracted data set, and producing new versions of the velocity map and the rotation curve. In neither case did the rotation curve show a decrease in gradient, or in peak value, so that we can safely discount an instrumental effect as responsible for them (Knapen et al. 2000). From a radius of 7″ (700 pc) out to 110 arcsec (some 11 kpc) the rotation curve remains flat, apart from deviations well confined in radius at ∼30″ and ∼50″ which occur where the streaming motions in the density wave system are strongest, and represent projected non-circular velocity components. The tangential velocity would be even flatter than our derived curve, which should be taken as a representation averaged in azimuth round the disc.

The position angle of the major axis remains essentially constant for galactocentric distances of more than 10″, with a value of 137°(±2°). A cut in the velocity map along the minor axis (at position angle 47°) reveals, effectively, a residual velocity structure in the inner part of the disc, which is not expected if this is the true kinematic minor axis, and if we are dealing exclusively with circular motion. The most reasonable interpretation of these significant systematic velocities is that they are non-circular, and associated with the star forming circumnuclear ring. A revised fit was performed, taking these non-circular

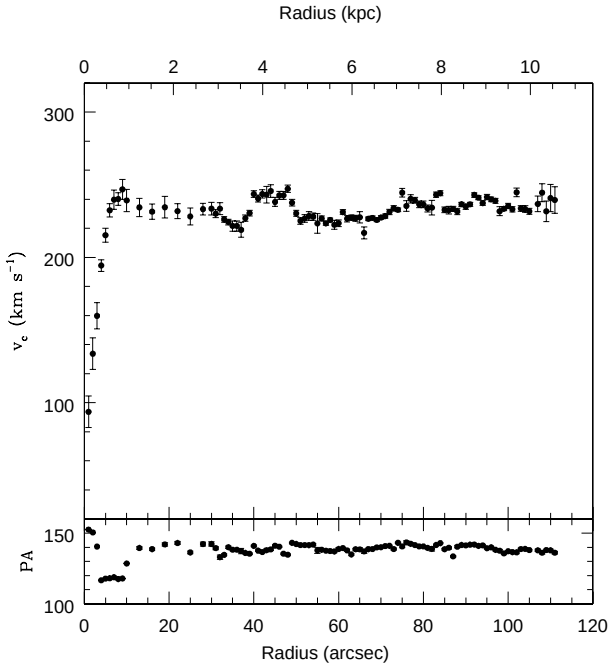

Fig. 10. Rotation curve (obtained from the 1.3″ resolution data cube) for NGC 6951 showing Hα velocities (upper graph) and computed major axis position angle (lower graph).

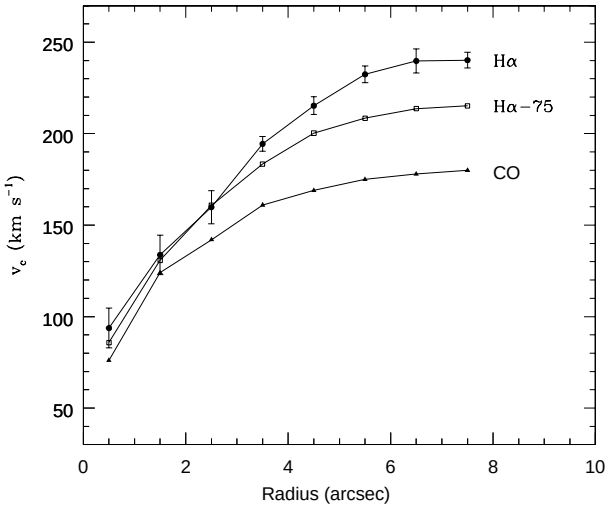

Fig. 11. Rotation curve derived from the Hα data set for the inner region of NGC 6951 (filled dots) and CO rotation curve from Kohno et al. (1999) (filled triangles). Also included (open squares) the Hα rotation curve when only points in the velocity fields at more than 75° from the minor axis are taken into account for the rotation curve fit.

components into account, yielding a significant variation in the position angle of the kinematic major axis, as shown in Fig. 10. A value of 119° was obtained for the zone between 2.5 and 7 arcsec from the centre; this may be compared with the value of 130° given for the circumnuclear zone by Kohno et al. (1999) based on their CO velocity field; this value is lower than the value across the disc by Márquez & Moles (1993) of 138° which agrees with our value of 137° presented here, but is significantly higher than our circumnuclear value, possibly due to the fact that we have better angular resolution in Hα. The clean constant value of the circumnuclear position angle shown in Fig. 10 leads us to infer that we might be dealing here with a disc rotating within the main disc, but decoupled from it, and not coplanar, or with a kinematic effect of an oval distorsion near the centre, or indeed due to a small bar through the nucleus. We will return to this point in more detail below. Finally we should note that the apparent behaviour of the curve beyond 105 arcsec radius cannot be taken as a basis for interpretation, since the S:N of the data makes them reliable only within this limit.

In Fig. 11 we show the internal portion of the Hα rotation curve, in comparison with the CO curve from Kohno et al. (1999). For a valid comparison we had smoothed our cube to the resolution of the CO observations.

There are two notable differences between the two curves: the CO curve rises more slowly that the Hα curve, and also reaches a lower maximum velocity. Noting that we are covering essentially the circumnuclear zone, we can attribute the differences either to non-circular motions, or to the geometrical displacement between the sites of CO and Hα emission in this region. Examination of the two velocity maps shows that the major discrepancies occur at the points of maximum star formation. At these points the velocity differences reach 50–70 km s^{-1} in the plane of the galaxy. In principle the Hα and CO should be measuring the kinematics of the same gas streams, since the young massive stars ionizing the gas which emits Hα should still be in the orbits of the molecular clouds from which they have formed. This suggests that the differences seen are probably due to the different distributions of the molecular and ionized gas. As a trial, to see whether this is a plausible, we plotted a revised Hα rotation curve, excluding those points at less than 75° from the minor axis, which is also plotted in Fig. 11. This should reduce effects due to non-circular motion, and relative displacements in the emission. The resulting curve has a reduced slope and maximum velocity, intermediate between those of the mean Hα curve, and the CO curve. An effect of this type was described by Rand (1993), and implies a significant problem in deriving the "true" rotation curve, i.e. the curve of material circulating purely under the central component of the gravitational field.

With the kinematic parameters of the curve we have computed the mass which yields a rigid body rotation curve, finding a value of, $M = 7.2 \times 10^9\ M_\odot$ out to $R = 0.7$ kpc (Burstein et al. 1982), the radius of maximum circular velocity.

5.3. Model velocity map, and residual velocity field

The radial velocity map in two dimensions reveals departures from circular motion, as we have seen, in Figs. 7–9. The two main types of non-circular motions are those associated with the arms, and those associated with the

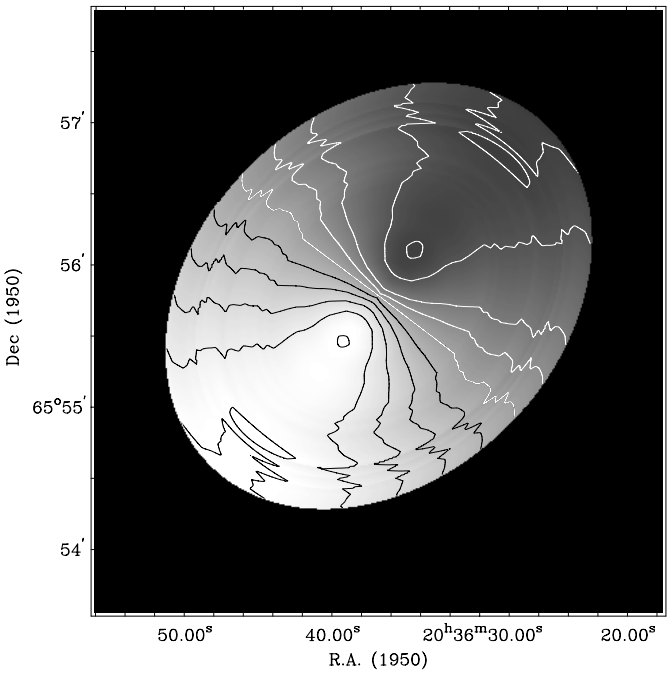

Fig. 12. Model rotational velocity map of NGC 6951, computed using fits to a set of inclined annuli (see text for more details). The isovels have a separation of 15 km s^{-1}.

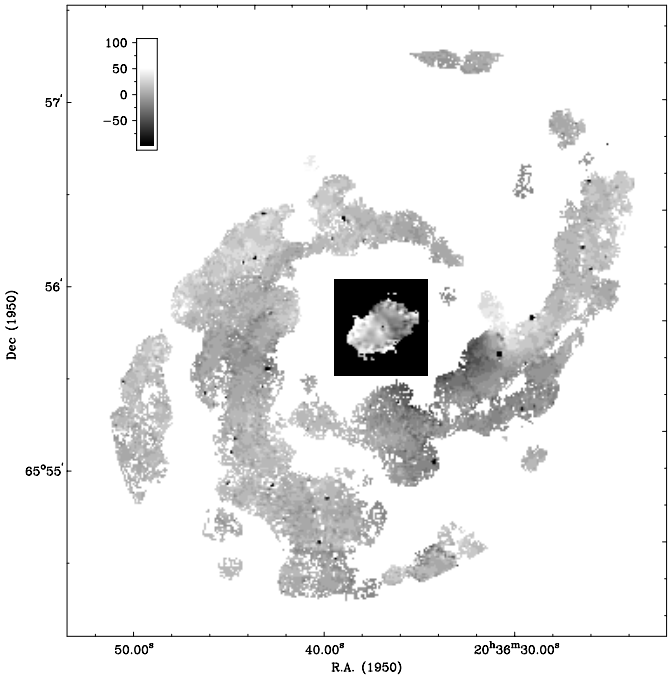

Fig. 13. Map of residual velocities for NGC 6951 obtained by subtracting off the two–dimensional model computed from the rotation curve from the observed velocity map.

bar. Theoretical models of galaxy dynamics predict the presence of gas streaming motions along spiral arms as part of the density wave system which causes them, and movement of the gas in the form of generally elliptical paths whose major axis is aligned with the axis of the bar, in barred galaxies. In order to bring out and quantify these non-circular motions, one needs to subtract off the circular velocity component. The way to do this in practice is to compute the velocity field due to this component as projected into the line of sight, and subtract this from the observed two dimensional velocity field. The circular velocity field obtained by rotating the mean rotation curve (the final rotation curve computed taking into account the non-circular motions at the central zone of the galaxy) about the nucleus, and projecting into the line of sight is shown in Fig. 12, and the map of residual non-circular velocities obtained by subtracting this field from the observed velocity field is shown in Fig. 13. The residual map for the whole disc is given in Fig. 13, and the circumnuclear zone with superposed residual isovel is displayed in greater detail in Fig. 14. These maps show the general distribution of the non–circular velocities, and where they have the highest amplitudes. A difficulty with this procedure is that any point on the mean rotation curve is produced by azimuthally averaging the observed radial velocities around an elliptical disc annulus, which implies that any strong departures from circularity will affect, albeit in a diluted fashion, the resulting mean, and thus also affecting the map of residuals. Although in some cases the non-circular motions possess a degree of axial symmetry, which leads to an effective cancellation of their amplitudes in the mean rotation curve, this is by no means always the case. The most accurate results are therefore contained in position–velocity diagrams, but as these are less easy to appreciate intuitively by all but the most hardened radioastronomers, we first discuss the non-circular components using the map of residuals. To minimize the inaccuracies in the rotation curve described here, we used a modified version, in which the position angle was held fixed at 137°, which minimized the effect of the non-circular velocities on the resulting two–dimensional circular velocity model.

Our initial interpretations are based in Fig. 13. Fixing our attention first on the spiral arms, we see that the residual velocities observed are not large, of order 20 km s^{-1}, positive or negative, except for certain restricted zones due to stronger streaming motions, which, with amplitudes of order 50 km s^{-1} are strong enough to be picked out in the "circular" velocity field. These are found in the NW arm, some 50″ from the nucleus, and in both the NW and SE arms, at some 25″ from the nucleus. Further motions can be seen within the zone around the bar, along its E and W edges, at some 35″ from the nucleus. These are all presumably directed within the plane of the galaxy, but in the overall residual map one can also see velocites related to the internal motions of the brightest HII regions, which represent large scale turbulence, and have components in all three Cartesian directions, for which there may be a dominant motion perpendicular to the plane, representing the "chimneys" proposed by Norman & Ikeuchi (1988) as accompanying phenomena to major OB associations.

In Fig. 14 we see that the regions within the circumnuclear zone where the departures from circular velocity are most marked are the regions of strong star formation

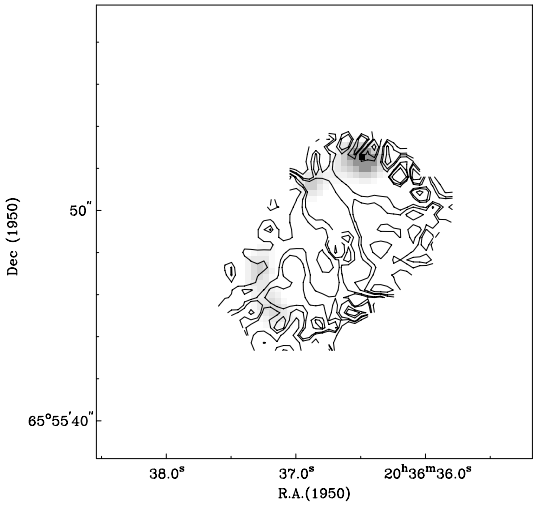

Fig. 14. Map of residual velocities of the central zone for NGC 6951 (intensity map with isocontours of residual velocity superposed).

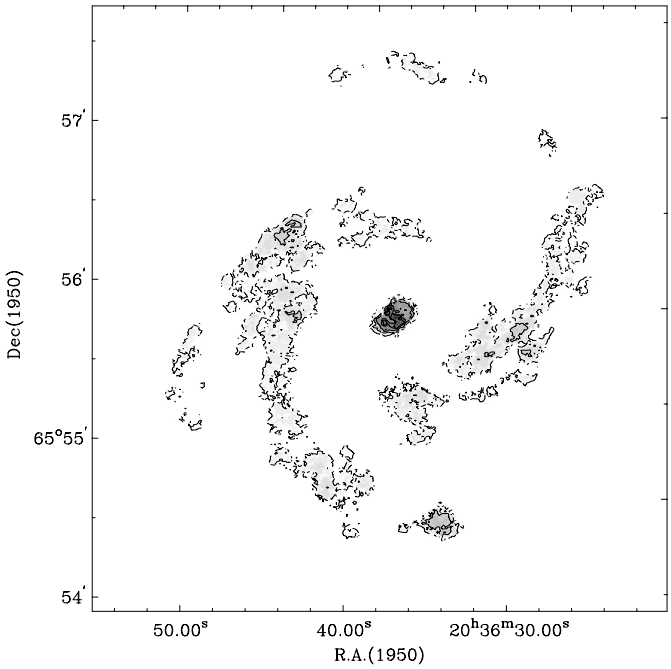

Fig. 15. Map of the velocity dispersion in the Hα emission of NGC 6951, with contours at 20, 35, 55, 80 and 100 km s^{-1} superposed. Darker shading corresponds to higher velocity dispersions.

towards the outside of the annulus, above all on its N and S edges, coinciding with the ends of the arms as picked out in CO (Kohno et al. 1999), and directly connected with the opposed dust lanes. The values of the residual velocities reach 50 km s^{-1} in these regions. If we assume that the spiral arms of NGC 6951 are trailing, and the dust lanes are situated at the leading edge of the bar, the SW part of the galaxy is the part nearer to us, so that the non-circular motions are due to radial flow of gas along the bar, a phenomenon long predicted in theoretical models (Roberts et al. 1979), and observed in a number of galaxies. As well as these strong velocity residuals, there are others nearer the nucleus, which could be related to the presence of an inner bar. Pérez et al. (2000) showed a variety of observational results indicating that NGC 6951 is a dynamically old object, which might harbour a fairly weak nuclear bar, which is not readily observed, but which drives gas towards the nucleus, according to the "bars within bars" scenario (Shlosman et al. 1989). Pérez et al (2000) do not find evidence for such an inner bar, and suggest that it might have been dissipated by the dynamical effects of the gas accumulating around the nucleus. However the non-circular velocities we find here could point to the continued presence of this small nuclear bar. The NW and SE ends of the proposed bar centred on RA = 20h36m43.72s Dec = +65°56′6.8″, and RA = 20h36m43.21s Dec = +65°56′8.2″ respectively, show respective positive and negative residual velocities, and the spiral arms show analogous behaviour, with a negative residual component centred at RA = 20h36m43.91s Dec = +65°56′6.5″ and a positive residual component centred at RA = 20h36m43.21s Dec = +65°56′8.2″. This is as expected for a twofold symmetric displacement from pure galactocentric rotation; the amplitudes of these non–circular components are of order 40 km s^{-1}.

5.4. The velocity dispersion map

As a final parameter which can be inferred from the data cube, we have produced a map of the second moment, i.e. of the velocity dispersion along the line of sight. This was derived using values for the gaussian half–width of the emission line fitted pixel by pixel. The maps in Figs. 15 and 16 are the velocity dispersion map (for the whole disc and the central region), but corrected at each position for non–kinematic broadening: instrumental, natural, and thermal. These corrections were made by subtracting in quadrature the line widths due to these three sources of broadening, according to the formula:

$$\sigma_{\rm obs} = \left[\sigma_{\rm N}^2 + \sigma_{\rm Ins}^2 + \sigma_{\rm t}^2 + \sigma_{\rm nt}^2\right]^{1/2} \quad (2)$$

where the observed line width is $\sigma_{\rm obs}$, the inferred kinematic non-thermal linewidth is $\sigma_{\rm nt}$, and the other three broadening terms are those described above. The natural line width, $\sigma_{\rm t}$, is essentially constant, with a value for hydrogen of 0.16 Å which is equivalent to 3 km s^{-1} (O'Dell & Townsley 1988). The instrumental width was found from the observed width of a line from the laboratory source used to produce the wavelength calibration cube. After checking that this cube did not show systematic structure due to calibration errors, we measured the velocity dispersion in the output line at 16.1 ($\pm$0.3) km s^{-1}, which we used as $\sigma_{\rm Ins}$. The thermal line-width $\sigma_{\rm t}$ was chosen assuming a temperature of 10^4 K for the ionized gas (Spitzer 1978; Osterbrock 1989), yielding a value of 9.1 km s^{-1}.

The resulting map of non-thermal dispersion is shown in Figs. 15 and 16. One can see that the highest dispersions

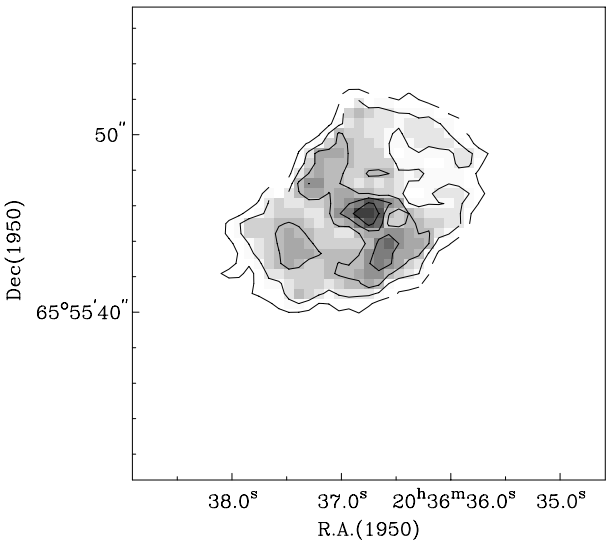

Fig. 16. Map of the velocity dispersion in the Hα emission of central zone of NGC 6951, with contours at 20, 35, 55, 80 and 100 km s^{-1} superposed. Darker shading corresponds to higher velocity dispersions.

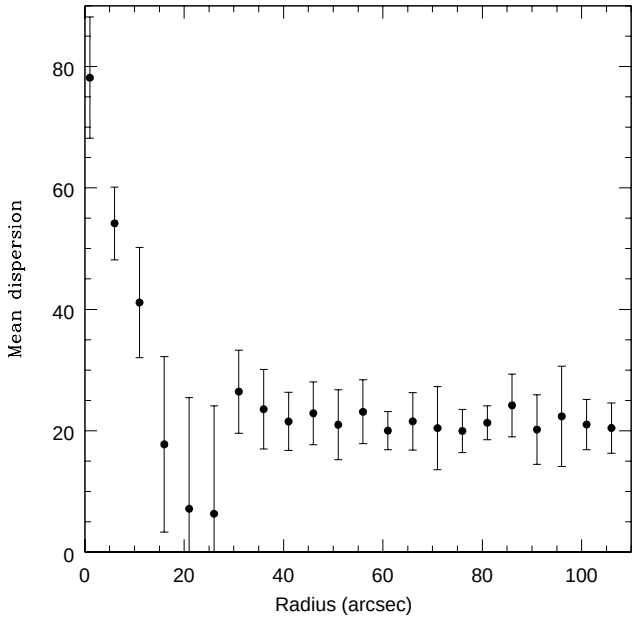

Fig. 17. Radial distribution of the velocity dispersion in annuli of width 5″.

are found in the circumnuclear zone, reaching values of 115–125 km s^{-1} in the centre. From this central maximum there is a systematic decline to 25–30 km s^{-1} in the outer part of the emitting annulus, with local peaks at around 55–60 km s^{-1} at the positions of the brightest HII regions.

These high dispersions in the central region are consistent with a continuous input of turbulent energy by the shocks produced where the stream lines in the gas crowd together, as suggested by Pérez et al. (2000), or with the injection of turbulent energy from the strong circumnuclear star formation region.

Over the disc in general we can see that the highest velocity dispersions correspond to the most luminous HII regions. A more detailed analysis, region by region, will be needed to quantify this relation (Relaño et al. 2001), but a quick look suggests that it will be qualitatively similar to those found for M100 and M101 (Rozas et al. 1998), in which the most luminous regions tend to be virialized, and with evidence for density bounding. As we can see in Fig. 17, the mean value for the dispersion of the Hα emission from the galaxy is some 22 km s^{-1}. The dispersion is found to be virtually constant outside a galactocentric radius of 30 arcsec, and the apparently low values in the range between 10″ and 30″ are not significant, since there is a markedly low mean emission level in this range. There are several possible mechanisms which could explain the constant value, including the conversion of galactic rotational energy to random cloud-cloud dispersion via viscosity (Combes & Becquaret 1997); or the conversion of stellar photon and wind energy to HII region turbulence.

6. The circumnuclear region of NGC 6951

In the central region of NGC 6951 we can pick out 8 hot spots in Hα (see Fig. 4, arranged within an annulus of some 135 pc in width, and at a distance of some 350 pc from the nucleus (a distance of 24.1 Mpc is used for the galaxy here). This kind of circumnuclear hot spots has been detected in a number of galaxies, since the initial work of Sersic & Pastoriza (1965, 1967); objects in which recent detailed work has been reported include NGC 4321 (Knapen et al. 2000), NGC 4314 (Benedict et al. 1996), NGC 3351, and NGC 5248 (Elmegreen et al. 1997). As shown by Elmegreen et al. (1999), this type of annulus forms the extension towards the nucleus of the two principal spiral arms of the galaxy, and the hot spots punctuate the edges of the resulting tightly wound system. As shown here, the spiral arms are also delineated by dust lanes, which cut the annulus and are projected inwards towards the nucleus. Inspection of an Hα image of NGC 6951 shows clearly that the central zone harbours concentrated formation of massive stars, and it is probable that the HII region population contains not only the highest luminous hot spots, but smaller regions too crowded to detect, and regions which have merged to form larger ones (Knapen et al. 2000).

As brought out earlier, the position angle of the major axis of the circumnuclear zone does not coincide with that found for the disc of the galaxy, which is compatible only with non-axisymmetric structure. As the geometrical parameters of the circumnuclear annulus: its position angle PA of 119° and its inclination angle i of 50°, do not coincide with the parameters of the main galaxy disc, we can infer that the annulus cannot be both circular and in the plane of the galaxy. We are left with two options: 1) the circumnuclear HII regions form a circular ring, inclined at some 8° to the plane of the galaxy or 2) the ring is not circular, but oval, in the plane of the galaxy, and with a radius which varies between 6″ and 9″. We first tested

the second possibility, using the kinematics to do so, in the form of the observed residual velocity field. We experimented with a kinematic model, in which we superposed a uniform contraction on the circular rotational motion, and checked to see how the residual velocities, $v_{\rm r}$, found using the best axisymmetric model, fit the observations when the position angle in the plane of galaxy is varied. Any radial velocity ($v_{\rm R}$), whether of expansion or contraction, should show up as a sinusoidal variation when projected along the line of sight, according to the formula:

$$v_{\rm r} = v_{\rm R} \sin({\rm PA}) \sin i. \quad (3)$$

We did not find good agreement using this modelling procedure. Nor did we find agreement when we tried to fit the dynamical predictions of an oval distorsion to the observed residual velocity field, and there are no photometric observations which would lead us to infer the presence of an oval dynamical distortion in the circumnuclear zone.

Because of these disagreements, we then checked the first possibility, which appears to suggest a more complex geometry, but in practice gives better agreement with observation. The kinematics supports this, and there is also geometrical evidence, noting that the brightest regions in the ring are situated all at one side, to the NE, while the fainter regions are concentrated in the SW. With an inclined ring this result could be due to dust in the plane of the galaxy, causing more extinction in the part of the ring below the plane.

The central zones of galaxies are places where resonances between the stellar orbital precession rates and the pattern speeds of bars tend to occur, at about the rotational velocity turnover radius (Shlosman 1999). The number of these inner resonances depends on the slope of the rotation curve, which depends on the axisymmetric component of the gravitational potential. If the conditions hold for the presence of one or more internal resonances the gas response is strongly affected, since the stream lines of the gas flow are forced to intersect and form twin shocks. These in turn cause the radial flow towards the nucleus, (normal in barred systems) to be slowed down, and gas accumulates between the outer and the inner internal resonances, with the resulting increase in the star formation rate in this zone (Schwarz 1984; Combes & Gerin 1985; Shlosman et al. 1989; Knapen et al. 1995). This scenario implies that there is a clear causal relation between the presence of multiple internal resonances and circumnuclear star forming annuli.

We carried out a standard analysis of the kinematics of NGC 6951 in order to find the positions of the principal resonances: the corotation radius and the Inner Lindblad Resonances (ILR's). From the rotation curve we computed the angular velocity $\Omega(r) = v(r)/r$, the epicyclic frequency, $k(r) = \{2[v(r)/r][v(r)/r + {\rm d}v(r)/{\rm d}r]\}^{0.5}$ and the function $\Omega - k/2$. The ILRs could then be found at the positions where the value of $\Omega - k/2$ equals the pattern speed, and the latter was measured at 42 km s^{-1} kpc^{-1}, assuming that the corotation radius is situated at the end of the bar. The radial length of the bar was taken from

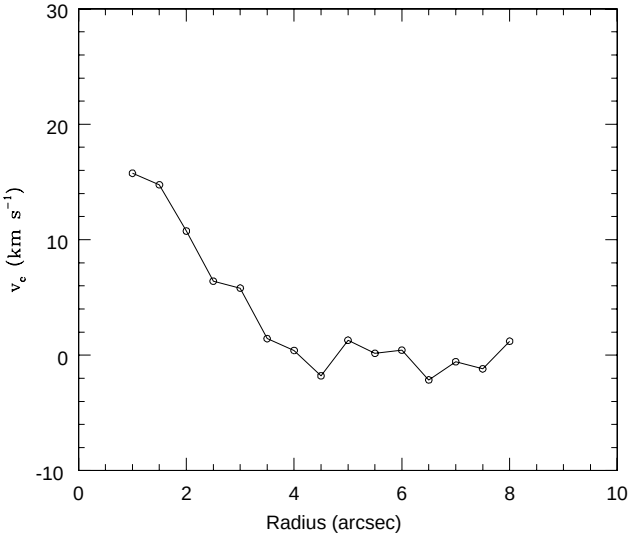

Fig. 18. Velocity profile in the central zone of NGC 6951, from the high resolution data cube, taken along the minor axis of the circumnuclear zone (PA = 29°).

Mulchaey et al. (1997) as 44″, which corresponds to two points on the $\Omega - k/2$ curve, and to the inference of two ILR's, an inner or IILR at 180 pc from the centre, and an outer, or OILR at 900 pc from the centre.

One might expect to find morphological evidence to corroborate our dynamical inference of an IILR at ∼180 pc from the centre. Published Hα images in the literature show structures within the inner 2″ (∼250 pc) so that the nuclear zone does not contain only a single point source. To help decipher this we obtained velocity profiles in the central zone at position angles PA = 119° and PA = 29°, respectively perpendicular to and parallel to the disc minor axis, and these reveal signs of specific velocity structure within the inner 250 pc. Figure 18 shows that the gas in the circumnuclear zone is in apparent counter-rotation with respect to the sense of rotation of the galaxy as a whole. A possible implication here is that there in this zone the geometry demands another position angle, different again from that in the annulus. If this were in fact the case, it would have a reasonable physical interpretation as being due to a decoupling of the gas within the IILR from the gas external to it. With a new fitting sequence to the velocity map in rings of width 0.5″ for the whole of the circumnuclear zone, we obtain a best fit position angle for the material inside the IILR of 153°, as shown in the lower panel of Fig. 19; the upper panel in the figure shows the rotation curve in this radial range. It is also possible that the inclination angle in this central zone differs from that of the annulus, but it is not possible to make valid simultaneous fits to the velocity and the inclination, so that we cannot confirm this conjecture in this way. Although the ring width we have used here equals the pixel size, and the number of points in the fit is small, it does appear that the inferred position angle close to the nucleus differs from that in the outer circumnuclear zone.

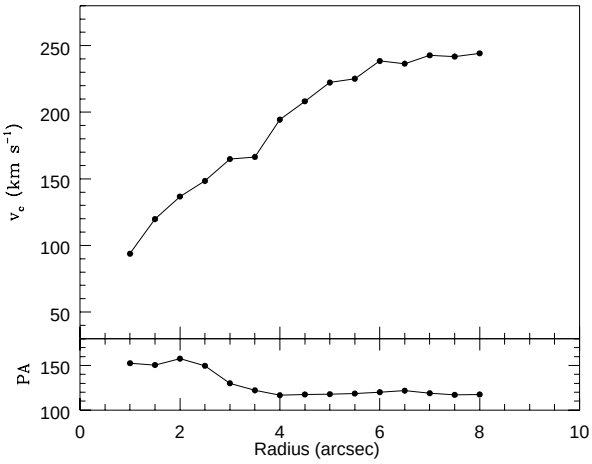

Fig. 19. Rotation curve of the central zone of NGC 6951 (upper panel) and position angle (lower panel).

We can offer an interpretation of the kinematics described above in terms of a set of nested discs within discs at the centre of NGC 6951. In this scenario the circumnuclear disc accumulates mass from the main disc at the OILR. This inflow continues through the IILR towards the nucleus, where another disc (or other rotating structure) is formed. The presence of an IILR in this system would allow a decoupling of the central structure from what we have termed the "circumnuclear annulus" (see Ferrarese & Ford 1999). A kinematic structure of this nature was put forward as a possibility for NGC 6951 by Pérez et al. (2000), but the spectroscopic data on which they based their conjecture was one-dimensional.

It is not, in general, safe to use moment maps to interpret kinematic features in regions of a galaxy where the profiles are not Gaussian, and may have multiple components. This is the case for NGC 6951, so we have gone on to produce a set of position-velocity diagrams along and parallel to the minor axis (we used a PA for the major axis of 119°, i.e. the nuclear value rather than the disc value, so that the minor axis PA is at 29°). These diagrams, in Fig. 20, do show that there is more than one velocity component in the central zone. Each panel in Fig. 20 shows the velocity as a function of distance, in arcsec, from the centre, either along the minor axis, or along a parallel axis; the plots are shown at intervals of 1″. The kinematic interpretation here is complicated by the high values of the velocity dispersion within the emitting HII regions around the centre, which tends to mask any streaming velocities. However we can see clearly in the figure two kinematic components offset in RA by +2″ and –2″, and with velocity offsets of 10–15 km s^{-1}. These could in fact be produced by a rotating component, and are consistent with the presence of a disc inside the IILR, very close to the nucleus. This goes some way to strengthening our claim about the presence of this disc, detected via the change in position angle, and velocity gradient shown in Fig. 19. This is also consistent, as suggested in Perez et al. (2000), with the morphology of the zone around the nucleus as revealed in HST images. However given the small scale of the features and the phenomenology, at the limit of what can be detected with our resolution, both angular and in velocity, we would not wish to claim more than a prima facie case for the presence of the inclined disc at the position angle and inclination angle described above. An alternative interpretation in terms of a circumnuclear counter-rotating bar, while offering a somewhat inferior fit, can in no way be ruled out at this stage. We can speculate no further here on this point, which would require higher resolution observations to clarify.

7. Conclusions

The principal outcomes of this study of the kinematics in the disc and the circumnuclear region of the ionized gas in the barred spiral NGC 6951 are as follows:

- We present a kinematic map in Hα, made with a Fabry-Perot system, extracting channel maps separated by a resolution interval of 17 km s^{-1}, and also a zeroth moment map, giving the integrated intensity, a first moment map, giving the velocity field, and a second moment map giving the velocity dispersion field, as well as a series of selected position-velocity diagrams to bring out specific kinematic features in chosen zones.
- Analysis of the velocity map reveals a disc in normal axisymmetric rotation, but with departures from circular motion in the arms, around the bar, and in the region of the nucleus. The velocity map yields a systemic velocity of 1422 km s^{-1}, and an inclination angle $i = 42°$, in agreement with previously published results.
- There is a strong concentration of Hα emission in the central zone of the galaxy, notably from an annulus in which strong massive star formation is taking place, marked by major HII region complexes. Outside this zone the Hα concentration is relatively weak, and traces out the spiral arms in an essentially symmetric configuration.
- Comparing the distribution of the Hα emission in the central zone with observations in CO and HCN, we find a better positional correlation with the HCN map, a phenomenon which has been noted previously in minor starbursts.
- Subtracting off a two-dimensional model obtained by rotating the mean rotation curve about the axis of rotation of the galaxy, in appropriate projection, from the observed two-dimensional velocity map we produce a map of residuals which gives a fair quantification of the non-circular velocity fields in NGC 6951. This shows clearly the streaming motions along the spiral arms, characteristic of the presence of density waves in a disc, and also gas flows along the main bar. We can also detect motions associated with flows from the most luminous HII regions, consistent with movement directed perpendicular to the galactic plane.

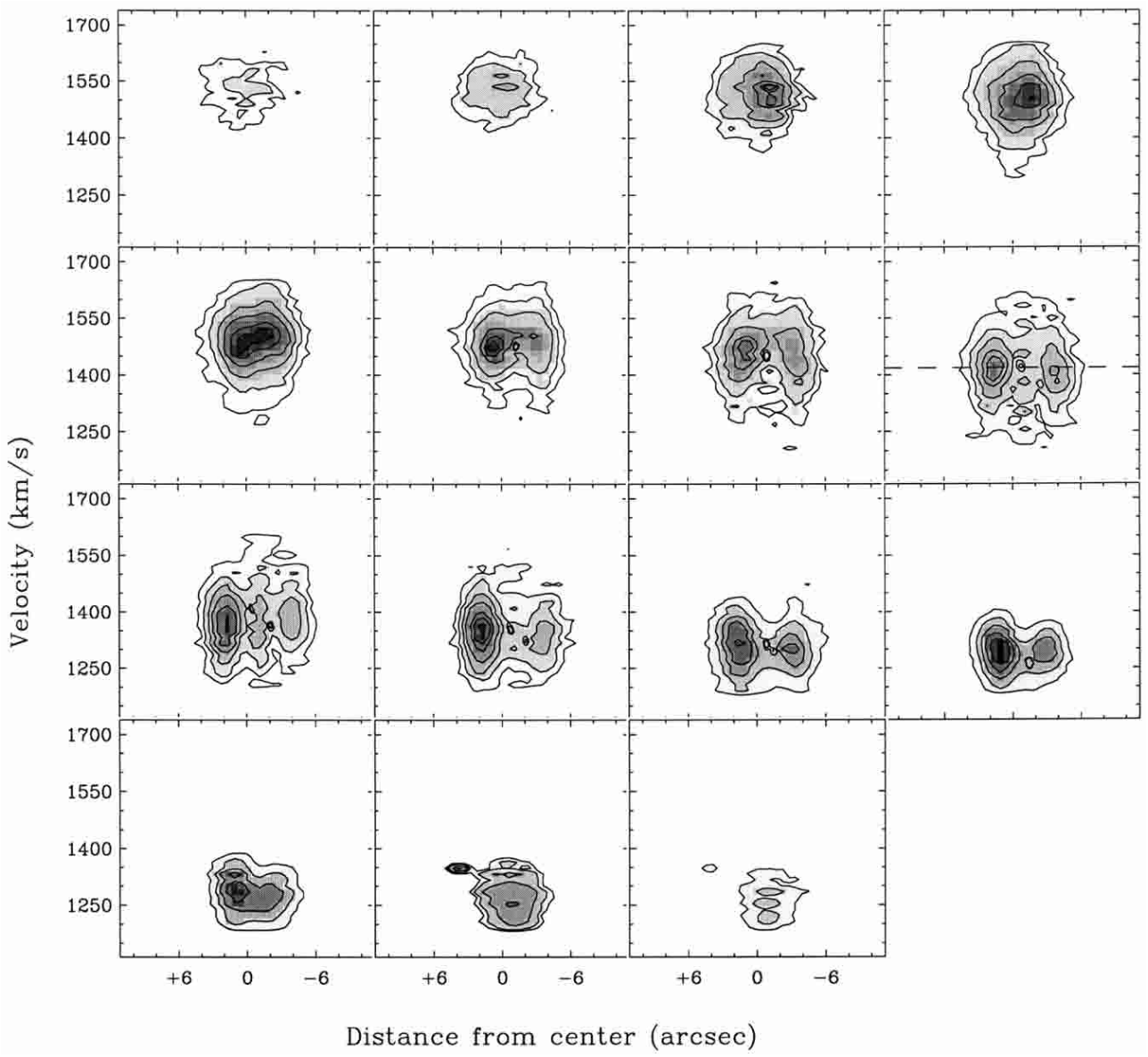

Fig. 20. Position velocity diagrams of the Hα emission along (panel indicated by a horizontal dashed line) and parallel to the minor axis in the central region of NGC 6951, position angle 29°. Panels to the left and above the minor axis panel are sections north of the minor axis, panels below are south. Sections are separated by 0.5″ but only every second diagram is shown. The systemic velocity of the galaxy is indicated by the horizontal line in the minor axis panel.

- The map of velocity dispersion shows that in the outer part of the disc, beyond some 30″ in radius, corresponding to some 3.5 kpc from the centre, the dispersion takes an essentially constant value of 22 km s^{-1}. The mean value rises sharply towards the nucleus, and individual emission peaks above the most luminous star forming regions show dispersions as high as 100 km s^{-1} in the circumnuclear annulus, and closer to the nucleus.
- Using a linear resonance analysis we determined the positions of two Inner Lindblad Resonances, at 900 pc and 180 pc from the centre respectively.
- Detailed analysis of the gas kinematics in the circumnuclear zone is consistent with observations of a series of nested discs, decoupled from one another, associated with the two ILR's. The position angles corresponding to this interpretation are given in Table 2.
- However we would not, on the basis of the present observations, wish to rule out the presence of a nuclear bar, whose potential can cause inflow of gas to the active nucleus, and which could also be consistent with the kinematic signatures detected close to the nucleus.

Table 2. NGC 6951: position angles.

Zone	Value
Global disc	137°
Circumnuclear region	119°
Nucleus	153°

Since bars of this sort tend to be dissipated by the dynamical effects of the central mass, the solution with a circumnuclear bar is perhaps the less probable, but data at higher resolution would be required to give a definitive answer.

Acknowledgements. The William Herschel Telescope is operated on the island of La Palma by the Royal Greenwich Observatory in the Spanish Observatorio del Roque de los Muchachos of the Instituto de Astrofísica de Canarias. This work has been partially supported by the Spanish DGICYT (Direccion General de Investigación Científica y Técnica) via grants PB94-1107, PB97-0219, and by the Spanish Ministry of Science and Technology, via grant AYA 2001-0435. This research has made use of the NASA/IPAC Extragalactic Database (NED) which is operated by the Jet Propulsion Laboratory, California Institute of Technology, under contract with the National Aeronautics and Space Administration. We are grateful to the referee, Dr. E. Pecontal, for meticulous revision of our paper, which has certainly improved it both in content and presentation.

References

Adams, T. F. 1977, ApJS, 33, 19
Arsenault, R. 1989, A&A, 217, 66
Athanassoula, E. 1992, MNRAS, 259, 345
Baiesi-Pillastrini, G. C. 1987, A&A, 172, 375
Barth, A. J., Ho, L. C., Filippenko, A. V., & Sargent, W. L. W. 1995, AJ, 110, 1009
Berentzen, I., Heller, C. H., Shlosman, I., & Fricke, K. 1998, MNRAS, 300, 49
Begeman, K. 1989, A&AS, 223, 554
Benedict, G. F., Smith, B. J., & Kenney, J. D. P. 1996, AJ, 111, 1861
Boer, B., & Schulz, H. 1993, A&A, 277, 397
Brosche, P. 1971, A&A, 13, 293
Burstein, D., Rubin, V. C., Thonnard, N., & Ford, W. K. 1982, ApJ, 253, 70
Buta, R., & Crocker, D. A. 1993, AJ, 105, 1344
Buta, R., & Combes, F. 1996, Fund. Cosmic Phys., 17, 95
Combes, F., & Gerin, M. 1985, A&A, 150, 327
Combes, F. 1988, in Galactic and Extragalactic Star Formation, ed. R. E. Pudritz, & M. Ficg (Dordrecht: Kluwer), 475
Combes, F., & Becquaret, J. F. 1997, A&A, 326, 554
Dahari, O. 1985, ApJS, 57, 643
Depree, C., Cecil, G., & Veilleux, S. 1991, BAS, 23, 1335
de Robertis, M. M., & Osterbrock, D. E. 1986, ApJ, 301, 727
de Vaucouleurs, G., de Vaucouleurs, A., Corwin, H. G., et al. 1991, Third Reference Catalogue of Bright Galaxies (Springer, New York)
Elmegreen, D. M., Elmegreen, B. G., Chromey, F. R., Hasselbacher, D. A., & Bissell, B. A. 1996, AJ, 111, 1980
Elmegreen, D. M., Chromey, F. R., Santos, M., & Marshall, D. 1997, AJ, 114, 1850
Elmegreen, D. M., Chromey, F. R., Sawyer, J. E., & Reinfeld, E. L. 1999, AJ, 118, 777
Ferrarese, L., & Ford, H. C. 1999, ApJ, 515, 583
Filippenko, A. V., & Sargent, W. L. W. 1985, ApJS, 57, 503
Forbes, D. A., Norris, R. P., Williger, G. M., & Smith, R. C. 1994b, AJ, 107, 984
Friedli, D., & Martinet, L. 1993, A&A, 277, 27
Friedli, D., Wozniak, H., Rieke, M., Martinet, L., & Bratschi, P. 1996, A&AS, 118, 461
González-Delgado, R. M., Pérez, E., Tadhunter, C., Vílchez, J. M., & Rodriguez-Espinosa, J. M. 1997, ApJS, 108, 155
Haynes, M. P., van Zee, L., Hogg, D. E., Roberts, M. S., & Maddalena, R. J. 1998, AJ, 115, 62
Ho, L. C., Filippenko, A. V., & Sargent, W. L. W. 1995, ApJS, 98, 477
Ho, L. C., Filippenko, A. V., & Sargent, W. L. W. 1997, ApJS, 112, 315
Hummel, E., van der Hulst, J. M., & Keel, W. C. 1987, A&A, 172, 32
Joseph, R. D., Meikle, W. P. S., Robertson, N. A., & Wright, G. S. 1984, MNRAS, 209, 11
Joseph, R. D., & Wright, G. S. 1985, MNRAS, 214, 87
Kenney, J. D. P., Wilson, C. D., Scoville, N. Z., Devereux, N. A., & Young, J. S. 1992, ApJ, 395, L79
Kennicutt, R. C. 1983, ApJ, 272, 54
Kennicutt, R. C., Edgar, B. K., & Hodge, P. W. 1989, ApJ, 337, 761
Kennicutt, R. C. 1994, in Mass–Transfer Induced Activity in Galaxies, ed. I. Shlosman (Cambridge University Press, Cambridge), 131
Kohno, K., Kawabe, R., & Vila–Vilaró, B. 1999, ApJ, 511, 157
Knapen, J. H., Beckman, J. E., Heller, C. H., Shlosman, I., & de Jong, R. S. 1995, ApJ, 454, 623
Knapen, J. H. 1997, MNRAS, 286, 403
Knapen, J. H., Shlosman, I., Heller, C. H., et al. 2000, ApJ, 528, 219
Laurikainen, E., & Moles, M. 1988, AJ, 96, 470
Laurikainen, E., & Moles, M. 1989, ApJ, 345, 176
Márquez, I., & Moles, M. 1993, AJ, 105, 2090
Moles, M., García-Pelayo, J. M., Masegosa, J., Aparicio, A., & Quintana, J. M. 1986, A&A, 152, 271
Mulchaey, J. S., Regan, M. W., & Kundu, A. 1997, ApJS, 110, 229
Muñoz-Tuñón, C., Vílchez, J. M., Castañeda, H., & Beckman, J. E. 1989, ApJS, 157, 165
Norman, C. A., & Ikeuchi, S. 1988, Lecture Notes in Physics (Springer-Verlag, Berlin, New York), 306
O'Dell, C. R., & Townsley, L. K. 1988, A&A, 198, 283
Osterbrock, D. E. 1989, Astrophysics of gaseous nebulae (Freeman, San Francisco)
Paglione, T. A. D., Tosaki, T., & Jackson, J. M. 1995, ApJ, 454, L117
Pérez, E., Márquez, I., Marrero, I., et al. 2000, A&A, 353, 893
Rand, R. J. 1993, ApJ, 410, 68
Relaño, M., Rozas, M., & Beckman, J. E. 2001, in preparation
Roberts, W. W., Huntley, J. M., & van Albada, G. D. 1979, ApJ, 233, 67
Rozas, M., Beckman, J. E., & Knapen, J. H. 1996a, A&A, 307, 735
Rozas, M., Knapen, J. H., & Beckman, J. E. 1996b, A&A, 312, 275
Rozas, M., Sabalisck, N., Beckman, J. E., & Knapen, J. H. 1998, A&A, 338, 15
Rozas, M., Zurita, A., Beckman, J. E., & Pérez, D. 2000, A&AS, 142, 259
Rubin, V. C., Burstein, D., Ford, W. K., & Thonnard, N. 1985, ApJ, 289, 81
Rubin, V. C., Kenney, J. D. P., & Young, J. S. 1997, AJ, 113, 1250
Saikia, D. J., Pedlar, A., Unger, S. W., et al. 1994, MNRAS, 270, 46

Saikia, D. J., Shastri, P., Cornwell, T. J., Junor, W., & Muxlow, T. W. B. 1989, JApA, 10, 203
Schwarz, M. P. 1984, A&A, 133, 222
Sérsic, J. L., & Pastoriza, M. G. 1965, PASP, 77, 287
Sérsic, J. L., & Pastoriza, M. 1967, PASP, 79, 152
Shen, J., & Lo, K. Y. 1995, ApJ, 334, L99
Shlosman, I., Frank, J., & Begelman, M. C. 1989, Nature, 338, 45
Shlosman, I. 1990, in Paired and Interacting Galaxies, ed. J. Sulentic, & W. Keel (Dordrecht: Kluwer), IAU Colloq., 124, 689
Shlosman, I. 1999, in The Evolution of Galaxies on Cosmological Timescales, ed. J. E. Beckman, & T. J. Mahoney (San Francisco: ASP), ASP Conf. Proc., 187, 100
Sofue, Y. 1996, ApJ, 458, 120
Sofue, Y., Tutui, Y., Honma, M., & Tomita, A. 1997b, AJ, 114, 2428
Spitzer, L. 1978, Physical Processes in the Interstellar Medium (Wiley, New York)
Tully, R. 1988, Nearby Galaxies Catalogue (Cambridge: Cambridge Univ. Press)
van der Kruit, P. C., & Shostak, G. S. 1982, A&A, 105, 351
Vila, M. B., Pedlar, A., Davies, R. D., Hummel, E., & Axon, D. J. 1990, MNRAS, 242, 379
Wilson, A. S., Helfer, T. T., Haniff, C. A., & Ward, M. J. 1991, ApJ, 381, 79
Wozniak, H., Friedli, D., Martinet, L., Martin, P., & Bratschi, P. 1995, A&AS, 111, 115
Zhang, X. 1996, ApJ, 457, 125